Atmos. Chem. Phys., 17, 10733–10741, 2017
https://doi.org/10.5194/acp-17-10733-2017

Atmospheric Chemistry and Physics
Open Access
EGU

Direct molecular-level characterization of different heterogeneous freezing modes on mica – Part 1

Ahmed Abdelmonem

Institute of Meteorology and Climate Research – Atmospheric Aerosol Research (IMKAAF), Karlsruhe Institute of Technology (KIT), 76344 Eggenstein-Leopoldshafen, Germany

Correspondence to: Ahmed Abdelmonem (ahmed.abdelmonem@kit.edu)

Received: 6 April 2017 – Discussion started: 20 April 2017
Revised: 3 August 2017 – Accepted: 7 August 2017 – Published: 13 September 2017

Abstract. The mechanisms behind heterogeneous ice nucleation are of fundamental importance to the prediction of the occurrence and properties of many cloud types, which influence climate and precipitation. Aerosol particles act as cloud condensation and freezing nuclei. The surface–water interaction of an ice nucleation particle plays a major, not well explored, role in its ice nucleation ability. This paper presents a real-time molecular-level comparison of different freezing modes on the surface of an atmospherically relevant mineral surface (mica) under varying supersaturation conditions using second-harmonic generation spectroscopy. Two sub-deposition nucleation modes were identified (one- and two-stage freezing). The nonlinear signal at the water–mica interface was found to drop following the formation of a thin film on the surface regardless of (1) the formed phase (liquid or ice) and (2) the freezing path (one or two step), indicating similar molecular structuring. The results also revealed a transient phase of ice at water–mica interfaces during freezing, which has a lifetime of around 1 min. Such information will have a significant impact on climate change, weather modification, and the tracing of water in hydrosphere studies.

1 Introduction

Clouds influence the energy budget by scattering sunlight and absorbing heat radiation from the earth and are therefore considered the major player in the climate system. Formation of ice changes cloud dynamics and microphysics because of the release of latent heat and the Bergeron–Findeisen process, respectively (Pruppacher and Klett, 1997). Ice nucleation in the atmosphere can be triggered heterogeneously by aerosol particles and ice-nucleating particles (INPs), or it occurs homogeneously at about −38 °C (Pruppacher and Klett, 1997). Cloud evolution depends not only on temperature and humidity but also on the abundance and surface characteristics of atmospheric aerosols. Understanding the factors that influence ice formation within clouds is a major unsolved and pressing problem in our understanding of climate (Slater et al., 2016). Field and laboratory experiments on cloud formation started decades ago (see Schaefer, 1949; DeMott et al., 2011; Hoose and Mohler, 2012, and references therein) and are ongoing. A wide variety of results and observations has been obtained in cloud microphysics, especially with respect to the ice nucleation ability of atmospheric aerosol particles and, hence, the mechanisms of cloud dynamics, precipitation formation, and interaction with incoming and outgoing radiation. Aerosol particles act as cloud condensation nuclei for liquid clouds, immersion or contact freezing nuclei for mixed-phase clouds, and heterogeneous deposition nuclei for ice (cirrus) clouds. Depending on whether water nucleates ice from the vapor or the supercooled liquid phase, ice nucleation is classified as deposition nucleation or immersion nucleation, respectively. Despite numerous investigations aimed at characterizing the effect of particle size and surface properties of the INP, there is a lack of information about the restructuring of water molecules on the surface of INPs around the heterogeneous freezing point.

In this paper, the discrimination between the different modes of the freezing of water on an ice-nucleating surface using nonlinear optical spectroscopy is demonstrated. Mica, a widely found layered clay mineral and one of the most prominent mineral surfaces due to its atomic flatness

and chemical inertness produced by perfect cleavage parallel to the 001 planes (Poppa and Elliot, 1971), was selected as a model surface in this study. However, the image of an inert and atomically smooth surface prepared by cleavage of muscovite mica in an ambient atmosphere is not quite correct (Christenson and Thomson, 2016). Surface analytical techniques found that the surface of muscovite mica cleaved in laboratory air, as is the case in this work, contains a water-soluble compound, potassium carbonate crystallites, which may cover a few tenths of a percent of the surface area (Christenson and Israelachvili, 1987). Nevertheless, definitive chemical analysis showing its presence is not yet available. However, the mobility of the potassium ions as potassium carbonate does not necessarily significantly affect any measurement of average surface properties as in the case of this work, and at high humidities the potassium will be widely dispersed across the surface. Those readers who are interested in more details on the nature of the mica surface in general and the air-cleaved mica surface in particular are referred to the review paper of Christenson and Thomson (2016) and papers cited therein.

Mica, as a natural particle, is believed to be among the most effective ice-nucleating minerals in the deposition mode (Eastwood et al., 2008; Mason and Maybank, 1958). An early study, which used a projection microscope and focused on the deposition nucleation of ice on freshly cleaved synthetic fluorophlogopite mica, which is similar in structure to muscovite but has the hydroxyl groups replaced by fluorine, revealed that there is no growth of ice until saturation with respect to water is reached (Layton and Harris, 1963). The authors concluded that at temperatures above $-40\,^{\circ}\mathrm{C}$, the growth of ice on mica should be a two-step process: a nucleus forms as water and then freezes. Experimental evidence of two-step nucleation was also provided by Campbell et al. (2013) using an optical microscope. With the help of a scanning optical microscope, they showed that the nucleation, of various organic liquids crystallizing from vapor on mica surfaces, favored specific nucleation sites with surface features such as cleavage steps, cracks, and pockets. However, they suggested that a supercooled liquid phase forms first and then freezes after it has grown to a size which thermodynamically favors the solid phase. These assumptions were based merely on thermodynamic observations (temperature and vapor supersaturation). A later study by the same group has confirmed the role of the surface features and the two-step process for organic liquids and strongly suggested a two-step process for water and ice (Campbell et al., 2017). Recent molecular dynamics (MD) simulations of deposition freezing revealed that water first deposits in the form of liquid clusters and then crystallizes isothermally from there (Lupi et al., 2014). So far, there has been no direct experimental evidence of two-step freezing based on probing the molecular structuring of water molecules next to the surface.

In this work, second-harmonic generation (SHG) in total internal reflection (TIR) geometry was used to probe the change in the degree of ordering of water on the surface of mica. Compared to sum-frequency generation (SFG), SHG is a powerful and simple surface-sensitive spectroscopic tool for studying molecules near surfaces and at interfaces (Shen, 1989b, 1989a). The amplitude and polarization of the generated field, as a function of the polarization of the incident fields, carry information on the abundance and structure of the interfacial molecules between two isotropic media (Jang et al., 2013; Rao et al., 2003; Zhuang et al., 1999). More details on SHG and SFG can be found in Sect. 2 and in the Supplement. In the system described here, the SHG signal originates in the nonresonant electric dipolar contribution of the interfacial molecules. The signal response relates to the overall arrangements of the interfacial entities (Fordyce et al., 2001; Goh et al., 1988; Luca et al., 1995) and is proportional to the incident field and the second-order nonlinear susceptibility $\chi^{(2)}$ of the interface. When the interface is charged, due to this charge, the static electric field can induce a third-order nonlinear polarization due to the contribution of the third-order nonlinear susceptibility $\chi^{(3)}$ of the solution (Ong et al., 1992; Zhao et al., 1993). In this work, the contribution of $\chi^{(3)}$ to the total SHG signal has been ignored because there was no significant change in the interface charge with temperature. The change in pH with temperature is known for neutral water (e.g., from pH 7 at 25 °C to pH 7.47 at 0 °C). In addition, this change does not mean that water becomes more alkaline at lower temperatures because, in the case of pure water and according to Le Châtelier's principle, there is always the same concentration of hydrogen and hydroxide ions and, hence, the water is still neutral (pH = pOH) even if its pH changes. The pH 7.47 at 0 °C is simply the new way of referencing neutral water pH at 0 °C. In addition, assuming that the surface potential has an influence on the background signal, this will not change even if the pH changes with temperature because the surface potential values of the muscovite basal plane (the surface under study) is pH independent in the range of pH 5.6 to 10 (Zhao et al., 2008).

The results provide new insight into heterogeneous freezing processes and show the suitability of the method for studying current issues relating to ice nucleation. Initially, I found that the SHG signal drops following the formation of a thin film regardless of whether the freezing path consists of one or two steps and with the initially formed phase, liquid or ice, indicating a similar molecular structuring. In addition, I observed a transient SHG signal after immersion freezing. The hygroscopicity of mica is expected to play a role in the described processes. The hygroscopicity and Langmuir isotherm studies on mica are available in literature but only for room temperature where the sample and environment are at equilibrium (Balmer et al., 2008; Beaglehole et al., 1991; Hu et al., 1995). Such studies at supercooled surfaces are worth doing and could be a topic of future work. An atomic force microscopy (AFM) study at 21 °C showed no water absorbed on the surface of mica at RH (relative humidity) = 18 % (Hu et al., 1995). The first uniform wa-

ter phase, of large two-dimensional islands with geometrical shapes in epitaxial relation with the underlaying mica lattice, was observed at RH = 28 %. The growth of this water phase is completed when the humidity reached between 40 and 50 %. In my experiments on mica it is not possible to detect sub-monolayers, at least at this stage, due to technical reasons mentioned later. In the presented work, only clear steps in the signal were considered.

2 Experimental setup

2.1 Materials and setup

All experiments were carried out using MilliQ water (18.2 MΩ cm). The total organic content in this water is below 4 ppb. Mica samples were obtained from Plano GmbH, Wetzlar, Germany. The mica samples were freshly cleaved parallel to the 001 plane in air right before use. The freshly cleaved mica exhibits a wetting surface (on which water was spreading visually). The SHG experiments were conducted using a femtosecond laser system (Solstice, Spectra Physics) with a fundamental beam of 800 nm wavelength, 3.5 mJ pulse energy, ∼ 80 fs pulse width, 1 kHz repetition rate, and a beam diameter of ∼ 2 mm at the interface. The supercooled SHG setup and the measuring cell are similar to those described in previous publications (Abdelmonem et al., 2015, 2017). Compared to the setup described in Abdelmonem et al. (2015), a single fundamental beam incident on the interface was used (Fig. 1) and the SM (S-polarized SHG/45°-polarized incident) polarization combination was measured. Figure 1 shows the sample and beam geometry. The polarization direction of the incident beam was controlled by a half-wave plate followed by a cube polarizer. The generated signal was collected using a photomultiplier tube (PMT) placed downstream of an optical system including band-pass filters for 400 nm and a polarization analyzer. A sapphire prism was used as an optical coupler to the surface of a thin mica substrate, the basal plane of which was exposed to liquid water or water vapor. The fundamental beam had an incident angle of 15° with the surface normal of the outer side of the prism. Under this geometry, the reflected fundamental (800 nm) and generated SHG (400 nm) beams co-propagate to the sapphire–air interface at the other side of the prism at which both beams are refracted at two different angles. Only the SHG signal was allowed to reach the detection path. Before starting the measurements, the polarization of the SHG signal generated from water at the surface was analyzed and found to have the expected maxima at S and P polarizations corresponding to an incident 45°-polarized light. The signal was quadratically dependent on the input power. To study mica in TIR geometry, an index matching gel (IMG) from Thorlabs (G608N3, RI ∼ 1.45186 at 800 nm) was used to fix the mica sample on the hypotenuse of the sapphire prism. The freezing point was not specified

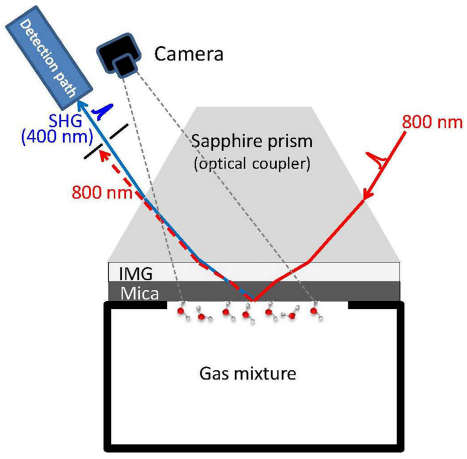

Figure 1. The sample and beams geometry. See text for details.

by the manufacturer but tested in the lab. The gel, at least, was not frozen until −45 °C. A detailed description of sample geometry and the selection of the IMG was published in Abdelmonem et al. (2015). Less than 15 % of the laser output power was coupled to the setup so as not to destroy the IMG. The fluctuation in the signal due to reducing the laser power limited the sensitivity of the system and it was not possible to monitor minor changes which may arise from pre-adsorption of sub-monolayers at temperatures higher than the dew point or freezing point.

A temperature-controlled environmental chamber developed in-house (Fig. 2) was integrated into the setup. A commercially available cold stage (Linkam model HFS-X350) was used after modifying the housing to accommodate the SHG setup. The sapphire prism was place in a copper adaptor which was fixed on the silver block of the Linkam cold stage. The substrate of interest was sealed to a circular opening of 8 mm in diameter in a teflon cell which was purged with the sample gas during the experiments. The cold stage can perform controlled heating and cooling ramps, applied to the silver block, at rates between 0.01 and 100 °C min^{-1}. The temperature stability of the cold stage is better than 0.1 K. The temperatures of the air inside the cell and the sapphire prism top and bottom were measured using four-wire Pt100 elements. The temperature of the probed spot on the surface was considered to be the average of the sample top and sample bottom temperatures. However, it should be emphasized that the exact onset condition of freezing is not the focus of this work, but the focus is rather the study of the qualitative behavior of water molecules during freezing on the different paths. During the experiments, the gas box was filled with N_2 gas to avoid condensation on the outer surfaces of the prism during cooling. The humid air pumped to the measuring cell was obtained by mixing dry gas and 100 % humid gas with different ratios at 21 °C using two mass flow controllers (Tylan 2900). The continuous flow of the gas (either dry or humid) during the experiment set the temperature in-

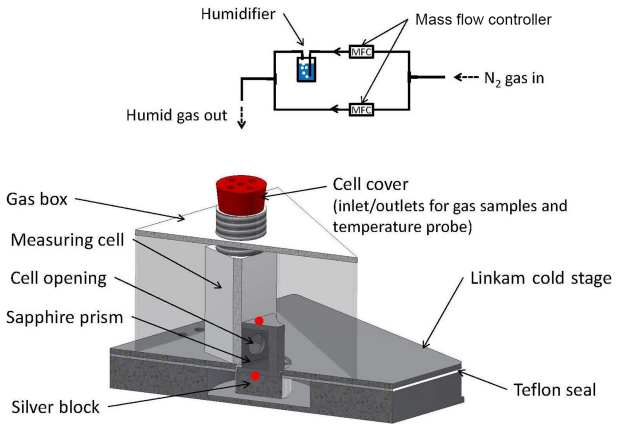

Figure 2. The temperature-controlled environmental chamber configuration and humidification and temperature sensors. The red dots are the position of the sample temperature sensors. There is a temperature sensor inside the measuring cell (not shown).

side the cell to 21 ± 0.5 °C. The corresponding fluctuation of the relative humidity was less than 0.2 %. The corresponding fluctuation in the dew point, at RH $= 5 \pm 0.2$ for instance, was ± 0.5 °C. The gas mixing ratio vs. RH was calibrated by setting a mixing ratio, cooling the sample, and recording the condensation/freezing temperature at which the reflectivity, at an angle equal to the critical angle of TIR for the air–mica interface, starts to drop due to the violation of the TIR condition. This temperature was used to define the corresponding RH using the Arden Buck equation.

The same method was used to differentiate between liquid film, liquid bulk, transient ice, and stable ice in this work. The border between a film at the solid–air interface and a bulk at the solid–water (or solid–ice) interface was defined experimentally by the point where the intensity of a TIR reflected light from the solid–air interface drops due to the violation of the TIR condition when the refractive index of the contact medium changes drastically from that of air ($n_a = 1$) to one of those of water or ice ($n_{w\,or\,i} > 1.3$). Whether the contact medium is liquid or ice, this was defined by the change in the light scattering, observed by a CCD camera (Guppy F-036 Allied Vision Technology with LINOS Macro-CCD Lens $0.14 \times (1:7)$ f4) placed close to the detection path (Fig. 1). After immersion freezing, there was a rapid increase in the signal and then a slow decrease. The maximum after the rapid increase was defined as the "transient ice" data point. After reaching a maximum, the signal decreased with time until it stabilized after a certain time. This stabilized signal was defined as the "stable ice" data point.

A control software was developed to adhere to a predefined temperature profile and to measure the SHG signal and the temperature of the substrate. Temperature profiles were repeated several times for each sample to test reproducibility. In each run, the sample was heated to 110 °C while purging with N_2 gas (99.9999 %) to evaporate any residual water; it was then cooled down to 0 °C at a rate of 10 °C min^{-1} and then down to the heterogeneous freezing point at a rate of 1 °C min^{-1}. This cooling profile was the same for all runs to allow a comparison. An experiment with a mica–N_2-gas interface was carried out to ensure that the change in the refractive indices of the sapphire prism, IMG, and mica substrate with temperature have no significant effect on the resulting SHG signal in the range of freezing temperatures observed in this work (Fig. S5 in the Supplement).

As mentioned above, the incident angle from air of the fundamental beam was adjusted to 15° with respect to the surface normal of the outer side of the sapphire prism. The corresponding incident angle on the mica–air or mica–water interface was $\sim 63.4°$, which is higher than the critical angles of TIR for mica–air ($\sim 39.7°$) and mica–water ($\sim 59.2°$) interfaces. This guaranteed a TIR condition regardless of any changes in the Fresnel factors caused by the change in refractive indices with changing temperature. The advantage of using an SM polarization combination is its dependence on only one nonvanishing nonlinear susceptibility tensor element (χ_{yyz}), (Shen, 1989a; Zhuang et al., 1999) at any working angle, which makes it a direct probe of the degree of order of the molecules at the interface.

The SHG signal is mainly produced by all polarizable species within the SHG-active region as long as the inversion symmetry is broken. The polarizable species at the surface of interest are the water molecules and the surface hydroxyls (OH). The contribution of water molecules is limited by the penetration depth inside the second medium (air, liquid water, or ice). Under the optical geometry described above, the calculated penetration depths are about 130, 328, and 253 nm for air, liquid water bulk, and ice bulk as contact media, respectively. Under the thermodynamical conditions of the presented work, the thickness of the ice (or water) layer should exceed 1 µm within 1 s after nucleation, which is far beyond the penetration depth of the evanescent field. Therefore, although the exact thickness cannot be determined in this setup it does not affect the probed signal by the two-interface problem because the second interface (ice–air or water–air) is not within the focal volume of the pump beam and the nonresonant signal comes exclusively from the first interface (water–solid or ice–solid). For the ice layer thickness, the reader is referred to the calculations of the growth velocity of a solidification front normal to the ice surface provided in the Supplement of the recent work of Kiselev et al. (2016). These calculations were taken from Libbrecht (2003, 2005). For calculations of growth due to condensation, the reader is referred to the Aerosol Calculator Program (Excel) by Paul Baron which is based on equations from Willeke and Baron (1993), Hinds (1999), and Baron and Willeke (2001). The signal was not collected until it became stabilized, and, therefore, it was assumed that the ice layer after deposition was uniform at the surface covered by the laser spot.

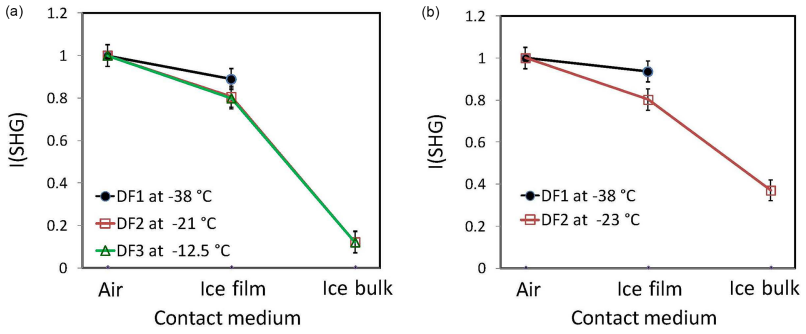

Figure 3. SHG intensity measured at the surfaces of mica **(a)** and sapphire **(b)** in contact with air, ice film, and ice bulk, collected in an SM polarization combination during the three different cooling cycles. DF1: sample cooled down first to −38 °C under dry N_2 gas, followed by pumping water vapor of RH = 5 % to the measuring cell. DF2: sample cooled down under flow of water vapor of RH = 5 %. DF3: sample cooled down under flow of water vapor of RH = 10 %. The signal is Fresnel-corrected and normalized to the air value. All connection lines between points serve to guide the eye.

3 Results and discussion

The RH of the purged gas was set to specific values in different runs to allow for different freezing modes on the surface of mica. Figure 3a shows the change in normalized Fresnel factor-corrected (see Supplement for details) SHG intensities under an SM polarization combination for deposition freezing (DF) at −38 °C (black solid line and circles), −21 °C (red solid line and empty squares), and at −12.5 °C (green solid line and empty triangles) labeled DF1, DF2, and DF3, respectively. In DF1, the cell was filled with N_2 gas and the sample was cooled down to a temperature (−38 °C) far below the dew point at RH = 5 % (−21 °C). At −38 °C, the cell was purged with humid air of RH ∼ 5 %. An ice film formed immediately on the surface, reflected by a drop in the SHG signal compared to that of the air–mica interface. In DF2 and DF3, the cell was purged continuously with humid air of RH = 5 and 11 %, respectively, and then cooled down until freezing and the growth of ice were observed on the surface. Deposition freezing and the formation of an ice film started at −21 and −12.5 °C for RH = 5 % (DF2) and 11 % (DF3), respectively. The results show a drop in the SHG signal with respect to the signal of the mica–air interface upon freezing for the three cases DF1, DF2, and DF3. However, the relative signal drop for DF1 differs from those of DF2 and DF3. DF2 and DF3 were observed at temperatures equal to the dew points at the preset RHs, indicating two-step nucleation: first condensation and then freezing. The coincidence of the SHG signals of the thin ice film formed in DF2 and DF3 indicates a similar degree of order of the water on the surface in two-step deposition freezing regardless of the onset temperature. This means that at temperatures above −38 °C, the growth of ice on mica is apparently a two-step process: water first condenses and then freezes. This confirms, at the molecular level, the two-stage nucleation hypothesis which suggests that a nucleus forms as a liquid cluster and then freezes (Layton and Harris, 1963; Lupi et al., 2014). Further pumping of the gas mixture to the measuring cell allows the growth of the ice film by diffusion. The resulting ice bulk shows a further drop in the signal for DF2 and DF3. This drop was not observed for DF1, thus indicating a major difference in the spectroscopic behavior of ice between one-step and two-step deposition freezing. To ensure that the lack of change in the SHG signal after the growth of an ice film to ice bulk in one-stage nucleation (DF1, Fig. 3a) is not an artifact, DF1 and DF2 were compared using a different system (sapphire–water interface; Fig. 3b). Figure 3b shows the change in SHG intensity at the surface of sapphire for DF at −38 (black solid line and circles) and at −23 °C (red solid line and empty squares), labeled DF1 and DF2, respectively. As in the case of mica, the drop in SHG intensity after the formation of an ice film was followed by another drop in the two-step freezing process (DF2) following further pumping of humid air of RH = 5 %, this was not the case in one-step (DF1) freezing.

Figure 4 shows three different freezing experiments at different RHs. The gas RH was adjusted to allow liquid condensation (LC) during cooling at temperatures higher than those of deposition freezing. Constant pumping of humid air at RH = 20, 30, and 40 % and cooling down resulted in the formation of stable liquid films at −3.5, 3, and 7 °C, respectively. At all RH values, the SHG signal drops down following the formation of a liquid film by LC. The relative drop in the signal with respect to the air signal is similar to that observed in the DF experiments (Fig. 3a). Comparing Figs. 3a and 4, the SHG signals are in the same range regardless of the film phase (liquid or ice). By further pumping humid air after LC, liquid bulk forms at the surface with a signal that is lower than that of the liquid film. This is mostly due to the contributions from the few secondary layers of the interfacial water. Further cooling of the sample in contact with liquid bulk causes water to freeze by immersion freezing (IF). The observed IF temperatures for IF1, IF2, and IF3 are similar and center around −11 ± 1 °C, which is within the range of

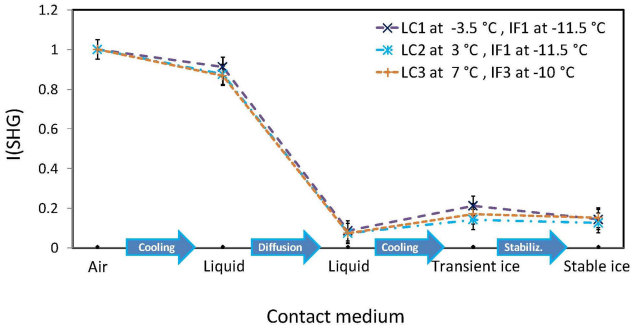

Figure 4. SHG intensity measured at the surface of mica in contact with air, liquid film, liquid bulk, transient ice bulk, and stable ice bulk, collected in an SM polarization combination during three different cooling cycles. LC1 IF1: sample cooled down under flow of water vapor of RH = 20 %. LC2 IF2: sample cooled down under flow of water vapor of RH = 30 %. LC3 IF3: sample cooled down under flow of water vapor of RH = 40 % (see text for details). The signal is Fresnel-corrected and normalized to the air value. Data before Fresnel correction are shown in Fig. S4 in the Supplement. All connection lines between points serve to guide the eye.

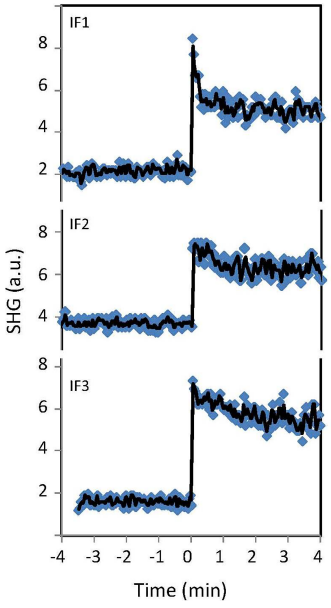

Figure 5. Typical variation in the SHG intensity around the immersion freezing points for IF1, IF2, and IF3 during the cooling experiments.

IF temperatures observed for the freezing of bulk water in contact with the surface of mica in former studies (Abdelmonem et al., 2015; Anim-Danso et al., 2016). IF produced a transient ice phase with an SHG intensity higher than that of the interfacial water of the bulk liquid. The lifetime of the transient phase is around 1 min (Fig. 5). The values of the SHG intensities plotted in Fig. 4 for transient ice bulk are the peak values found on the transient curves shown in Fig. 5 after Fresnel factor corrections and normalization to the mica–air signal. The transient phase may have had peak values higher than those obtained from Fig. 5, but they were not detected due to the fast signal decay right after nucleation and the limited time resolution of signal detection of about 2.5 s. A transient phase lasting for several minutes was reported very recently by Lovering et al. (2107) using SFG at a water–silica interface. They suggested a transient existence of stacking-disordered (non-centrosymmetric) ice during the freezing process at water–mineral interfaces. Anim-Danso et al. (2016) also observed such transient ice lasting for a few tens of seconds in SFG experiments at a high-pH (9.8) solution–sapphire interface. They suggested that charge transfer and the stitching bilayer are perturbed at high pH, which leads to a decrease in SFG intensity. The present work shows that the transient ice occurs at neutral pH on a mica surface and has a significant nonresonant component, which is observable with the simple SHG technique. The lifetime of the transient phase apparently depends on the substrate and probably on the liquid-bulk size and might play a role in the ice nucleation ability of the surface. However, this requires a comparative study involving different substrates, which will be subject of future work.

Finally, an explanation is warranted as to why there is a drop, rather than an increase, in the signal upon adsorption of water (or ice) on the surface (of either mica or sapphire). The SHG response reflects the overall arrangements of the polar entities at the interface between two isotropic media (Fordyce et al., 2001; Goh et al., 1988; Luca et al., 1995). This signal intensity is expected to increase when a single (or a few non-centrosymmetric) layer(s) of water or ice is (are) formed at (or added to) the surface, while SHG intensity decreases upon deposition freezing, condensation, and the growth of liquid layers by diffusion as can be seen in Figs. 3 and 4. One expectation could be phase interference between two signals originating from two different interfacial entities of opposite dipole moments. The possible contributors could be surface hydroxyls, pre-adsorbed water (films), and the added water. The surface hydroxyls can probably be ruled out, since mica-basal planes based on structural considerations should not have such groups, while sapphire-basal planes do. Thus pre-adsorbed water would be the more reasonable option. Such water films have actually been proposed on sapphire basal planes based on experimental data (Lützenkirchen et al., 2010) and reported in MD simulations (Argyris et al., 2011). This scenario, which may explain the decrease in SHG intensity upon deposition freezing, condensation, and the growth of liquid layers, involves the preexistence of a 2-D bilayer of water on the surface. This 2-D bilayer has the ordered structure of the water monolayer, which greatly enhances the numbers of H bonds inside the monolayer. This in turn reduces the likelihood of H-bond formation between the water molecules of this monolayer with

other molecules, a phenomenon which makes a hydrophilic surface hydrophobic (Wang et al., 2009; Hu and Michaelides, 2007; Ranea et al., 2009). Adjacent layers would then be comparable to those on hydrophobic surfaces and could yield the signal interference that is observed. Clearly, the drop in signal merits further investigation, in particular since pre-adsorbed water films are not necessarily identical for mica and sapphire. In particular the mica surface exhibits a quite complex interfacial hydration structure (Cheng et al., 2001).

4 Conclusions

In summary, a simple SHG setup was used to discriminate and describe three different freezing paths on the surface of mica. The results provide decisive evidence for, and confirm, at the molecular level, the previous speculations about the existence of two-stage deposition ice nucleation at temperatures above −38 °C. One-step and two-step deposition freezing of a thin film of ice show a water structure similar to that of a thin film of liquid water. When liquid bulk freezes at the surface by immersion freezing, there is a transient non-centrosymmetric ice phase of a highly nonresonant SHG signal. The lifetime of the transient phase is suggested to be substrate-dependent and expected to affect ice nucleation efficiency. The presented results open up new horizons for the role of aerosol surfaces in promoting and stabilizing heterogeneous ice nucleation. They provide novel molecular-level insight into different ice nucleation regimes using a simple spectroscopic technique. Investigating the structuring of water molecules upon freezing next to solid surfaces is crucial to many scientific areas, such as atmospheric physics and chemistry, hydrology, and environmental and industrial applications.

This work demonstrates the value of investigating different ice nucleation processes and water structuring upon freezing at the molecular-level using SHG spectroscopy. The paper is intended to serve as the basis of future complementary studies involving other surfaces and other techniques to precisely investigate the layer thickness, the surface morphology effect, the cooling rates, etc. The difficulty of characterizing monolayer films arose from the use of the IMG, which required reducing the power. An alternative would be to approach the surface from the air side which then has the disadvantage of a weak SHG signal and the two-interface problem. These are challenges which will be tackled in future work.

Data availability. The data used in this study are available from the corresponding author upon request (ahmed.abdelmonem@kit.edu).

Information about the Supplement

The Supplement comprises SHG and SFG theoretical background and data acquisition and Fresnel factors correction.

The Supplement related to this article is available online at https://doi.org/10.5194/acp-17-10733-2017-supplement.

Competing interests. The author declares that he has no conflict of interest.

Acknowledgements. The work is funded by the German Research Foundation (DFG, AB 604/1-1). The SHG setup was funded by the competence area "Earth and Environment" of KIT (start-up budget 2012). The author is grateful to Johannes Lützenkirchen and Alexei Kiselev for the scientific discussions on surface properties and ice growth, respectively, and to Thomas Leisner, Claudia Linke, and Maike Schröder from KIT for their support. The editor thanks Hugo Christenson and two anonymous reviewers for their assistance in evaluating this paper.

The article processing charges for this open-access publication were covered by a Research Centre of the Helmholtz Association.

Edited by: Daniel Knopf
Reviewed by: Hugo Christenson and two anonymous referees

References

Abdelmonem, A., Lützenkirchen, J., and Leisner, T.: Probing ice-nucleation processes on the molecular level using second harmonic generation spectroscopy, Atmos. Meas. Tech., 8, 3519–3526, https://doi.org/10.5194/amt-8-3519-2015, 2015.

Abdelmonem, A., Backus, E. H. G., Hoffmann, N., Sánchez, M. A., Cyran, J. D., Kiselev, A., and Bonn, M.: Surface-charge-induced orientation of interfacial water suppresses heterogeneous ice nucleation on α-alumina (0001), Atmos. Chem. Phys., 17, 7827–7837, https://doi.org/10.5194/acp-17-7827-2017, 2017.

Anim-Danso, E., Zhang, Y., and Dhinojwala, A.: Surface charge affects the structure of interfacial ice, J. Phys. Chem. C, 120, 3741–3748, https://doi.org/10.1021/acs.jpcc.5b08371, 2016.

Argyris, D., Ho, T., Cole, D. R., and Striolo, A.: Molecular dynamics studies of interfacial water at the alumina surface, J. Phys. Chem. C, 115, 2038–2046, https://doi.org/10.1021/jp109244c, 2011.

Balmer, T. E., Christenson, H. K., Spencer, N. D., and Heuberger, M.: The effect of surface ions on water adsorption to mica, Langmuir, 24, 1566–1569, https://doi.org/10.1021/la702391m, 2008.

Baron, P. A. and Willeke, K.: Aerosol Measurement: Principles, Techniques, and Applications, 2nd Edn., edited by: Sons, J., Wiley-Interscience, New York, 2001.

Beaglehole, D., Radlinska, E. Z., Ninham, B. W., and Christenson, H. K.: Inadequacy of Lifshitz theory for thin liquid films, Phys. Rev. Lett., 66, 2084–2087, 1991.

Campbell, J. M., Meldrum, F. C., and Christenson, H. K.: Characterization of preferred crystal nucleation sites on mica surfaces, Cryst. Growth Des., 13, 1915–1925, https://doi.org/10.1021/cg301715n, 2013.

Campbell, J. M., Meldrum, F. C., and Christenson, H. K.: Observing the formation of ice and organic crystals in active sites, P. Natl. Acad. Sci. USA, 114, 810–815, https://doi.org/10.1073/pnas.1617717114, 2017.

Cheng, L., Fenter, P., Nagy, K. L., Schlegel, M. L., and Sturchio, N. C.: Molecular-scale density oscillations in water adjacent to a mica surface, Phys. Rev. Lett., 87, 156103, https://doi.org/10.1103/PhysRevLett.87.156103, 2001.

Christenson, H. K. and Israelachvili, J. N.: Growth of ionic crystallites on exposed surfaces, J. Colloid. Interf. Sci., 117, 576–577, https://doi.org/10.1016/0021-9797(87)90420-6, 1987.

Christenson, H. K. and Thomson, N. H.: The nature of the air-cleaved mica surface, Surf. Sci. Rep., 71, 367–390, https://doi.org/10.1016/j.surfrep.2016.03.001, 2016.

DeMott, P. J., Möhler, O., Stetzer, O., Vali, G., Levin, Z., Petters, M. D., Murakami, M., Leisner, T., Bundke, U., Klein, H., Kanji, Z. A., Cotton, R., Jones, H., Benz, S., Brinkmann, M., Rzesanke, D., Saathoff, H., Nicolet, M., Saito, A., Nillius, B., Bingemer, H., Abbatt, J., Ardon, K., Ganor, E., Georgakopoulos, D. G., and Saunders, C.: Resurgence in ice nuclei measurement research, B. Am. Meteorol. Soc., 92, 1623–1635, https://doi.org/10.1175/2011bams3119.1, 2011.

Eastwood, M. L., Cremel, S., Gehrke, C., Girard, E., and Bertram, A. K.: Ice nucleation on mineral dust particles: onset conditions, nucleation rates and contact angles, J. Geophys. Res.-Atmos., 113, 203-201–203-209, https://doi.org/10.1029/2008jd010639, 2008.

Fordyce, A. J., Bullock, W. J., Timson, A. J., Haslam, S., Spencer-Smith, R. D., Alexander, A., and Frey, J. G.: The temperature dependence of surface second-harmonic generation from the air-water interface, Mol. Phys., 99, 677–687, https://doi.org/10.1080/00268970010030022, 2001.

Goh, M. C., Hicks, J. M., Kemnitz, K., Pinto, G. R., Heinz, T. F., Eisenthal, K. B., and Bhattacharyya, K.: Absolute orientation of water molecules at the neat water surface, J. Phys. Chem., 92, 5074–5075, https://doi.org/10.1021/j100329a003, 1988.

Hinds, W. C.: Aerosol Technology: Properties, Behavior, and Measurement of Airborne Particles, 2nd Edn., Wiley-Interscience, New York, 1999.

Hoose, C. and Möhler, O.: Heterogeneous ice nucleation on atmospheric aerosols: a review of results from laboratory experiments, Atmos. Chem. Phys., 12, 9817–9854, https://doi.org/10.5194/acp-12-9817-2012, 2012.

Hu, J., Xiao, X.-D., Ogletree, D. F., and Salmeron, M.: Imaging the condensation and evaporation of molecularly thin films of water with nanometer resolution, Science, 268, 267–269, https://doi.org/10.1126/science.268.5208.267, 1995.

Hu, X. L. and Michaelides, A.: Ice formation on kaolinite: lattice match or amphoterism?, Surf. Sci., 601, 5378–5381, https://doi.org/10.1016/j.susc.2007.09.012, 2007.

Jang, J. H., Lydiatt, F., Lindsay, R., and Baldelli, S.: Quantitative orientation analysis by sum frequency generation in the presence of near-resonant background signal: acetonitrile on rutile TiO_2 (110), J. Phys. Chem. A, 117, 6288–6302, https://doi.org/10.1021/jp401019p, 2013.

Kiselev, A., Bachmann, F., Pedevilla, P., Cox, S. J., Michaelides, A., Gerthsen, D., and Leisner, T.: Active sites in heterogeneous ice nucleation – the example of K-rich feldspars, Science, 355, 367–371, https://doi.org/10.1126/science.aai8034, 2016.

Layton, R. G. and Harris, F. S.: Nucleation of ice on mica, J. Atmos. Sci., 20, 142–148, https://doi.org/10.1175/1520-0469(1963)020<0142:noiom>2.0.co;2, 1963.

Libbrecht, K.: Growth rates of the principal facets of ice between $-10\,^{\circ}C$ and $-40\,^{\circ}C$, J. Cryst. Growth, 247, 530–540, https://doi.org/10.1016/S0022-0248(02)01996-6, 2003.

Libbrecht, K. G.: The physics of snow crystals, Rep. Prog. Phys., 68, 855, https://doi.org/10.1088/0034-4885/68/4/R03, 2005.

Lovering, K. A., Bertram, A. K., and Chou, K. C.: Transient phase of ice observed by sum frequency generation at the water/mineral interface during freezing, J. Phys. Chem. Lett., 8, 871–875, https://doi.org/10.1021/acs.jpclett.6b02920, 2017.

Luca, A. A. T., Hebert, P., Brevet, P. F., and Girault, H. H.: Surface second-harmonic generation at air/solvent and solvent/solvent interfaces, J. Chem. Soc. Faraday T., 91, 1763–1768, https://doi.org/10.1039/ft9959101763, 1995.

Lupi, L., Kastelowitz, N., and Molinero, V.: Vapor deposition of water on graphitic surfaces: formation of amorphous ice, bilayer ice, ice I, and liquid water, J. Chem. Phys., 141, 18C508, https://doi.org/10.1063/1.4895543, 2014.

Lützenkirchen, J., Zimmermann, R., Preočanin, T., Filby, A., Kupcik, T., Küttner, D., Abdelmonem, A., Schild, D., Rabung, T., Plaschke, M., Brandenstein, F., Werner, C., and Geckeis, H.: An attempt to explain bimodal behaviour of the sapphire c-plane electrolyte interface, Adv. Colloid Interfac., 157, 61–74, https://doi.org/10.1016/j.cis.2010.03.003, 2010.

Mason, B. J. and Maybank, J.: Ice-nucleating properties of some natural mineral dusts, Q. J. Roy. Meteor. Soc., 84, 235–241, https://doi.org/10.1002/qj.49708436104, 1958.

Ong, S., Zhao, X., and Eisenthal, K. B.: Polarization of water molecules at a charged interface: second harmonic studies of the silica/water interface, Chem. Phys. Lett., 191, 327–335, https://doi.org/10.1016/0009-2614(92)85309-X, 1992.

Poppa, H. and Elliot, A. G.: The surface composition of Mica substrates, Surf. Sci., 24, 149–163, https://doi.org/10.1016/0039-6028(71)90225-1, 1971.

Pruppacher, H. R. and Klett, J. D.: Microphysics of Clouds and Precipitation, 2nd edn., Atmospheric and Oceanographic Sciences Library, 18, Kluwer Academic Publishers, Dordrecht, Boston, 954 pp., 1997.

Ranea, V. A., Carmichael, I., and Schneider, W. F.: DFT investigation of intermediate steps in the hydrolysis of α-Al_2O_3(0001), J. Phys. Chem. C, 113, 2149–2158, https://doi.org/10.1021/jp8069892, 2009.

Rao, Y., Tao, Y.-S., and Wang, H.-F.: Quantitative analysis of orientational order in the molecular monolayer by surface second harmonic generation, J. Chem. Phys., 119, 5226–5236, https://doi.org/10.1063/1.1597195, 2003.

Schaefer, V. J.: The formation of ice crystals in the laboratory and the atmosphere, Chem. Rev., 44, 291–320, https://doi.org/10.1021/cr60138a004, 1949.

Shen, Y. R.: Optical second harmonic generation at interfaces, Annu. Rev. Phys. Chem., 40, 327–350, https://doi.org/10.1146/annurev.pc.40.100189.001551, 1989a.

Shen, Y. R.: Surface properties probed by second-harmonic and sum-frequency generation, Nature, 337, 519–525, https://doi.org/10.1038/337519a0, 1989b.

Slater, B., Michaelides, A., Salzmann, C. G., and Lohmann, U.: A blue-sky approach to understanding cloud formation, B. Am. Meteorol. Soc., 97, 1797–1802, https://doi.org/10.1175/bams-d-15-00131.1, 2016.

Wang, C., Lu, H., Wang, Z., Xiu, P., Zhou, B., Zuo, G., Wan, R., Hu, J., and Fang, H.: Stable liquid water droplet on a water monolayer formed at room temperature on ionic model substrates, Phys. Rev. Lett., 103, 137801, https://doi.org/10.1103/PhysRevLett.103.137801, 2009.

Willeke, K. and Baron, P.: Aerosol Measurement: Principles, Techniques, and Applications, edited by: Klaus Willeke, P. A. B., Van Nostrand Reinhold, New York, 1993.

Zhao, X., Ong, S., and Eisenthal, K. B.: Polarization of water molecules at a charged interface. Second harmonic studies of charged monolayers at the air/water interface, Chem. Phys. Lett., 202, 513–520, https://doi.org/10.1016/0009-2614(93)90041-X, 1993.

Zhao, H., Bhattacharjee, S., Chow, R., Wallace, D., Masliyah, J. H., and Xu, Z.: Probing Surface Charge Potentials of Clay Basal Planes and Edges by Direct Force Measurements, Langmuir, 24, 12899–12910, https://doi.org/10.1021/la802112h, 2008.

Zhuang, X., Miranda, P. B., Kim, D., and Shen, Y. R.: Mapping molecular orientation and conformation at interfaces by surface nonlinear optics, Phys. Rev. B, 59, 12632–12640, https://doi.org/10.1103/PhysRevB.59.12632, 1999.